Finite Element Simulation in Superplastic forming of Friction Stir Welded Aluminium Alloy 6061-T6

P.Ganesh[1,*], V.S. Senthil Kumar[2]

[1]Assistant Professor, Department of Production Technology, Madras Institute of Technology, Chrompet Anna University, Chennai 600044, India.
[2]Associate Professor, Department of Mechanical Engineering, College of Engineering, Guindy Anna University, Chennai 600025, India.

Abstract: Superplasticity in materials is the ability of materials to achieve large elongation only under specific conditions of temperature and strain rate. Superplastic Forming (SPF) is an important industrial process that has found application in sheet metal forming in the aerospace and automotive industries. Friction Stir Welding (FSW) is a solid state joining process that can alter the grain structure of the parent material. FSW process is an effective tool to refine the grain structure of the sheet metal and enhance their Superplasticity. Friction Stir Welding was used to join Superplastic AA 6061-T6 sheets. The Finite Element Simulation was performed for the Superplastic Forming of the Friction Stir Welded joints to evaluate the thinning and formability of AA 6061-T6 for hemispherical shape. The commercially available Finite Element Software ABAQUS was used to execute these simulations.

Keywords: Superplastic forming, friction stir welding, AA 6061-T6, finite element analysis.

1. Introduction

Aluminum (Al) alloys are receiving increasing interest in Aerospace industry principally because of their light weight: among structural materials, Al alloys have the low density and offer the highest potential for saving weight, especially in areas transportation components are in use. In these applications, the increasing demand for lightweight alloys, in particular for Al alloys and the inability of conventional forming techniques to effectively form these alloys make Superplastic Forming (SPF) an attractive forming technique. Extremely complex shapes can be manufactured by SPF. The application of the Blow Forming (BF) process is considering light metallic alloys such as aluminium, titanium and magnesium ones, some of which are hard to form using conventional conditions. The BF process consists in the application of a forming gas (e.g. air, argon) pressure on the blank at an elevated temperature that is forced in a die cavity. SPF has the advantage of forming components with large and complex shape, in a single operation, to a near net shape, reduce forming time and tooling cost, enhanced dimensional accuracy.

However, SPF with BF application for metals has not been used in the industry, owing to the high cost of the process and raw materials, which made this type of process globally less competitive compared with other conventional technologies. In order to overcome these limits, high strain rate superplasticity (HSRSP) and Friction Stir Welding (FSW) have been developed [10]. FSW is a relatively new way to perform welding operation in solid-state conditions. In FSW, the rotating tool is inserted in to the material and after dwell time, it moves along the joint line. Friction between the tool and the workpiece generates heat which reduces the flow stress of material around the rotating pin and tool shoulder and then the weld joint is produced by material flow from the advancing side to the retreating side of the weldment [9]. FSW has been successfully applied in the joining of aluminum, magnesium and titanium alloys.

An attempt has been made in combining the two processes (FSW-SPF), to study the effect of different friction stir welding rates on the microstructural evaluation, tensile testing, superplastic formability and superplastic thinning behavior of AA 6061-T6 superplastic sheets were investigated.

2. Experimental Work

The 3 mm thick AA 6061-T6 rolled plates was used for the present study. The Fig. 1 shows the schematic picture of the tool geometry used for the present FSW process. The shoulder face was designed as a concave cone while the inside angle of the rotating tool was about 82°. Table 1 shows the design parameters of the tool. The composition of the aluminum alloy is given in Table 2. Single pass welding was used to fabricate the butt joints. A non-consumable rotating tool made of M2 high speed steel with a hardness of 52 HRC was used to fabricate FSW joint. The welding tool was kept perpendicular to the workpiece. The selected range of tool rotating speed was 500, 710 and 1000 rpm and speed of travel was varied from 40 to 80 mm/min. The plates were clamped as shown in Fig. 2.
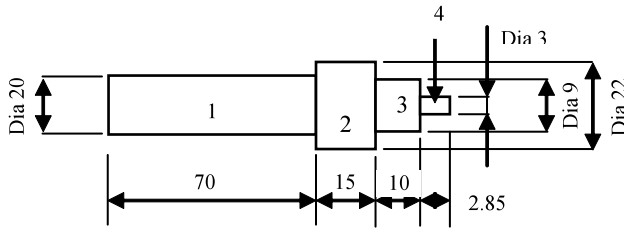
Fig. 1 Schematic illustration of the tool used in the present study; 1. Tool shank, 2. Tool head, 3. Tool shoulder, 4. Tool pin (All Dimensions are in mm).

Table 1 Design parameters of the FSW tool

Process parameter	Values
Tool shoulder diameter, D mm)	9
Pin diameter, d (mm)	3
Tool pin length, L (mm)	2.85
Tool inclined angle (^{o})	0
Tool shank diameter (mm)	20
Tool head diameter (mm)	22

Table 2 Chemical Composition of AA 6061 Alloy in wt%.

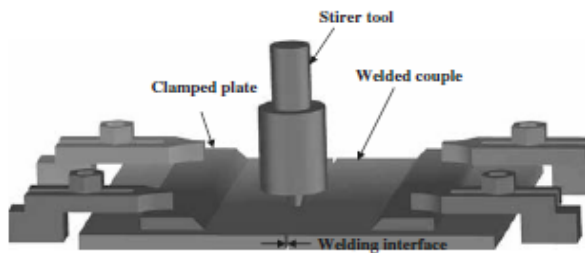| Al	Zn	Mg	Cu	Fe	Ti	Si	Mn
Balance	0.001	0.952	0.258	0.100	0.032	0.615	0.033

Fig. 2 Experimental setup of FSW.

The microstructural studies were made utilizing optical and scanning electron microscopy. After welding, the samples were sectioned normal to the welding direction and then prepared by grinding disks and polished and finally etched with Keller's reagent: 150mL H_2O, 3 mL HNO_3, 6 mL HCl, and 6 mL HF [9].

The superplastic behavior of the welded sheets was characterized through conducting uniaxial hot tensile testing using specimens cut along and across to the welding directions. The superplastic tensile specimen gage length, width, and thickness were 25, 6 and 2 mm, respectively. Reported total strain (elongation-to-fracture) for the after welding (500, 710 and 1000 rpm) was based on the average of at least two tests. The strain rate

sensitivity was approximated at several strain values from tests run at different constant strain rates.

The specimens were prepared from the FSW component as per the SPF die requirements. The specimens were blow formed to the hemispherical die shape at 450-500°C.

3. Results
3.1 Microstructural Evolution

The microstructure show in Fig. 3, the Annealed matrix of the alloy 6061 which has been cold worked (rolled). The microstructure shows the particles of Mg_2Si particles along with some particles of Fe_3SiAl_2 that has been broken up due to rolling process and formed along the direction of the rolling. Base metal of AA 6061-T6 contains coarse and elongated grains with uniformly distributed very fine precipitates. The Photo-micrograph shows the interface junction of the weld and the alloy 6061.The 6061 alloy has finer grains of Mg_2Si particles without orientation, shown in Fig. 4.
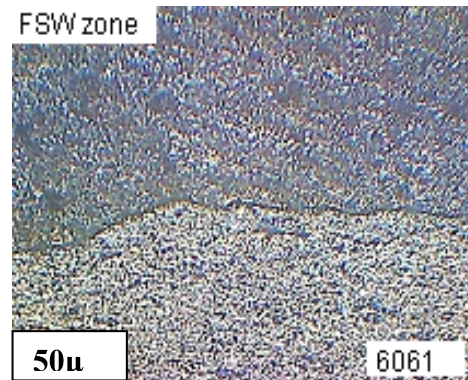

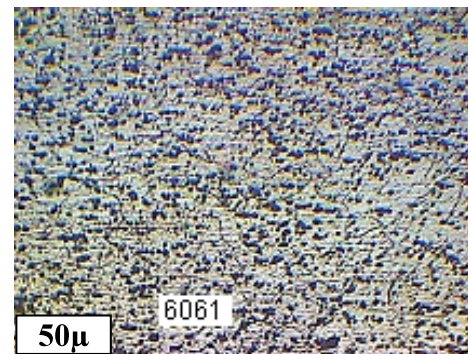Fig. 3 Microstructure of Base metal AA6061-T6.

Fig. 4 Microstructure of 6061-weld zone interface.

The matrix shows the microstructure of the weld zone. Fine grains of complex of Mg_2Si and with insoluble (Fe, Mn) Al_6 particles precipitated. There is a significant breakup of $MgZn_2$ particles, subsequently creating a uniform distribution of finer $MgZn_2$ particles in the α-aluminium matrix. It is due to the stirring action at plastic condition of the metal during FSW.

The weld region of FSW contains very fine grains and this is due to dynamic recrystallization that occurred during FSW process. FSW zone with thermo

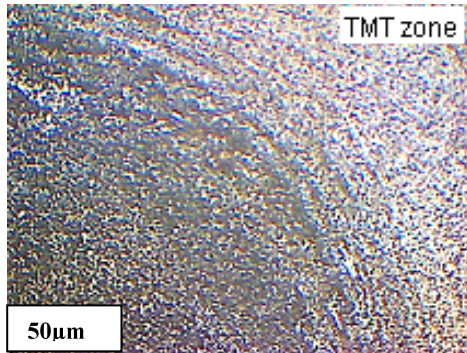mechanically formed ring like structures commonly known as onion rings is shown in Fig. 5.

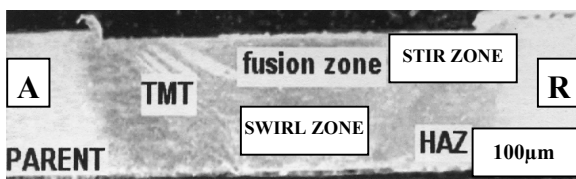Fig. 5 Onion Rings of 6061-weld zone interface.

Fig. 6 Optical micrographs showing the flow pattern in the nuggets after Friction Stir Welding.

Microstructural investigation using optical microscopy for the welded sheets within the weld nugget for all three welding speeds revealed the formation of similar macro and microstructures with slight variations. Accordingly, the sheets welded at 500, 710 and 1000 rpm were chosen for detailed analysis in the current section. Based on evidence that the heat input to the weld increases with decreasing welding rate using the same rotational speed.

The advancing side (AS) is on the left and the retreating side (RS) is on the right as shown in Fig.6. The microstructurally developed regions can be divided into 4 distinct zones: the stir zone along the weld centerline, a swirl zone extending towards the advancing side of the tool and within the stir zone, a thermomechanically affected zone (TMT) on either sides of the weld and a heat affected zone (HAZ) surrounding the TMT.

In general, friction stir welding produced grain sizes that varied between 2.6, 2.2, 3.6 and 4.5 μm at different locations across the weld nugget.

3.2 Tensile Properties

The superplastic behavior of the base metal and the FSW material welded at 500, 710, and 1000 rpm was investigated at a temperature of 450 °C and tensile strain rates of 3.36×10^{-4} s^{-1}. Estimates of true-stress and true-strain were determined from force and elongation measurements using the assumptions of constant volume and uniform cross-sectional area change. Fig. 7 shows typical stress-strain curves behavior at 450 °C and a strain rate of 3.36×10^{-4} s^{-1} for all three welded joint conditions.
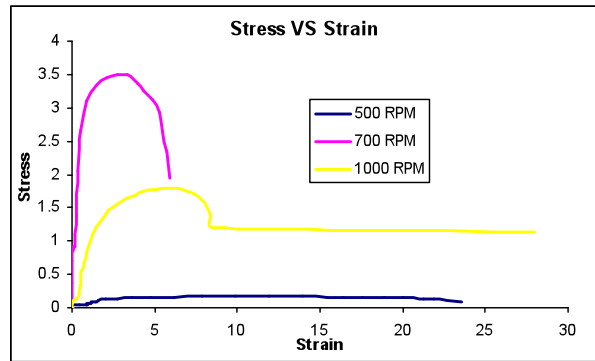

Fig. 7 Stress-Strain Superplastic Behavior of FSW at 500, 700 & 1000 rpm along the welding direction at strain rate of 3.36×10^{-4} s^{-1}.

Table 3 Hot Tensile Test Results

S.NO	PROP.	500 RPM		700 RPM		1000 RPM	
		ACR.	ALO.	ACR.	ALO.	ACR.	ALO.
1	UTM (N/mm²)	104	82	82	68	70	70
2	ELON. (%)	26	44	30	47.5	44.3	51
3	YIELD STRE. (N/mm²)	92	63	69	24	62	121

From the hot tensile test result in Table 3 shows that the ultimate tensile point decreases with increase in FSW rpm and the percentage of elongation increase in increase in FSW rpm. The hot tensile test specimens along and across the welded region can be visualized in Fig.8.
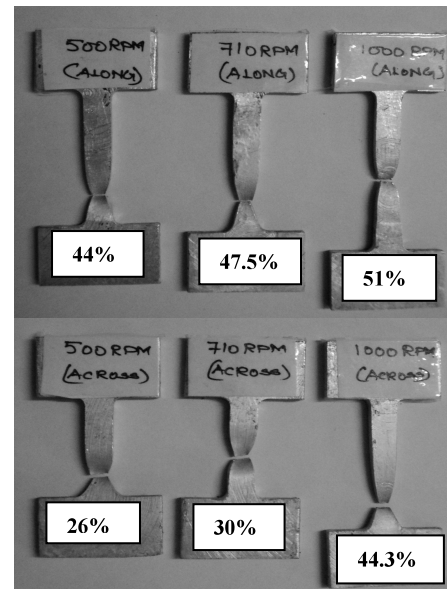

Fig. 8 Friction Stir Welding Superplastic Tensile Test coupons are shown after Stretching (Elongation) the FSW zone (along and across the weld zone).

4. Superplastic Behavior

The Superplastic behavior of Friction stir welded sheets welded at 500, 710 and 1000 rpm was investigated at a temperature of 450 ^{o}C and strain rate of 3.36 X 10^{-4} s^{-1}. The FSW-SPF were die formed in to hemispherical dome shape. The thickness variation along the cross section of the hemispherical dome is given in Table 4.

Table 4 Thickness variation along the cross section of Hemispherical Domes in mm

COMPO NENT	TRAIL NO.	BLANK THICK (mm)	THICKNESS AT THE SECTION (mm)			
			1	2	3	4
FSW- SPF	1	2	1.87	1.50	1.07	0.86
	2	2	1.81	1.80	1.40	1.03

Table 5 Dome heights FSW - SPF components

FSW- SPF	TEMP.	PRESS .	FORMING TIME	DOME HEIGHT
(RPM)	(^{o}C)	(Bar)	(Min)	(mm)
500	450	1 – 4.5	45	18.4
710	450	1 – 4.5	45	18.5
1000	450	1 – 4.5	50	25.2

The dome height values of FSW-SPF at various FSW tool rotational speed is given in Table 5. The various dome height formed by die forming process is shown in Fig.9. Fig.10. shows the schematic sketch of the Superplastic die forming (blow forming).
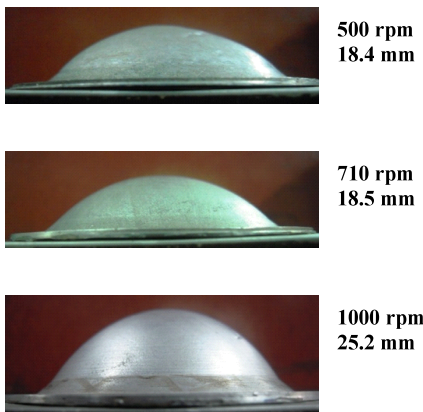

**500 rpm
18.4 mm**

**710 rpm
18.5 mm**

**1000 rpm
25.2 mm**

Fig. 9 Superplastic Behavior of FSW-SPF

5. Procedure For Determining Materials Data From The Inflation Test

The procedure for determining material parameters from Superplastic inflation test [4,5] shown in Fig. 11. Under the given constant pressure, the heights of the dome are measured by an LVDT device and recorded as a function of time.

Grid circles of diameter d_0 (2.5mm) laser etched on the sheets were employed to measure strain levels in each test [8]. During forming the laser etched circles were distorted into ellipses and/or larger circles.
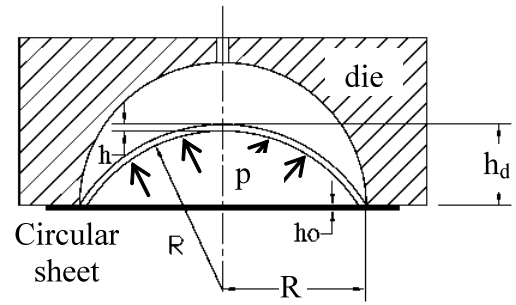

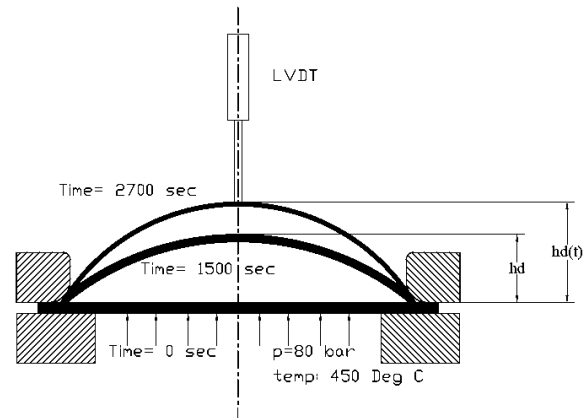Fig. 10 Superplastic Blow Forming (die forming).
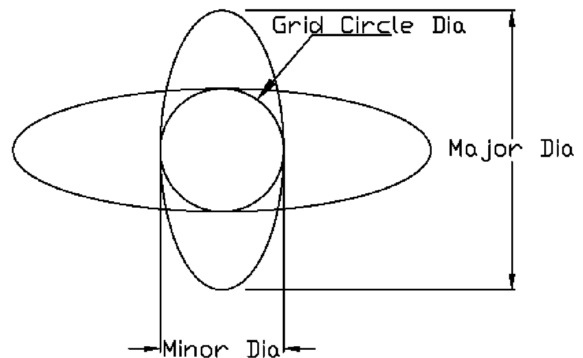

Fig. 11 Superplastic free-inflation process.

Fig. 12 Major and Minor Dia. Measurement.

Measurements of the major, d_1 and minor, d_2, diameters after deformation were made to determine the principal strains; the principal strain directions and distorted grids are given in Fig. 12. The principal strains, effective strain and strain rates can then be expressed as [1,4,5]

$$\varepsilon_1 = In\left(\frac{d_1}{d_0}\right) \qquad (1)$$

$$\varepsilon_2 = In\left(\frac{d_2}{d_0}\right) \qquad (2)$$

$$\varepsilon_3 = In \left(\frac{h}{h_0}\right) \tag{3}$$

$$\bar{\varepsilon} = \left[\frac{2}{3}\left(\varepsilon_1^2 + \varepsilon_2^2 + \varepsilon_3^2\right)\right]^{1/2} \tag{4}$$

$$\dot{\varepsilon} = \frac{\bar{\varepsilon}}{t} \tag{5}$$

where

h_0 : Original thickness of the sheet (mm)

h : Thickness of the deformed sheet (mm)

$\varepsilon_{1,2,3}$: Principle strain in directions 1,2 and 3

$\bar{\varepsilon}$: Effective strain

$\dot{\varepsilon}$: effective strain rate

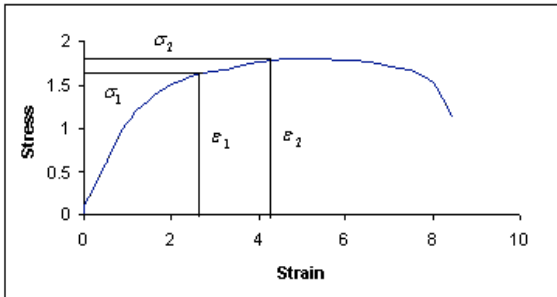t : forming time (sec)

K : Material constant

Fig. 13 Constitutive equation from flow curve ($h_d(t)$: Height function of time).

The equivalent stress is defined as

$$\sigma = \frac{1}{\sqrt{2}} \left[\left(\sigma_1 - \sigma_2\right) + \left(\sigma_2 \square \sigma_3\right) + \left(\sigma_3 \square \sigma_1\right)\right]^{1/2} \tag{6}$$

Table 6 Geometrical dimensions of the die and sheet

Parameter	Dimensions
Sheet radius (mm)	73
Die entry radius (mm)	3
Thickness of the sheet (mm)	2
Radius of the die (mm)	27

Assuming that there is no variation of stress through the thickness of a thin-walled pressure vessel, the hoop stress σ can be related to the applied pressure p by

$$\sigma = \frac{pR}{2h} \tag{7}$$

From the geometry shown in Fig. 10, it is found that

$$R^2 = R_d^2 + (R - h_d)^2 \tag{8}$$

where R_d is the die radius,

$$R = \frac{R_d^2 + h_d^2}{2h_d} \tag{9}$$

The instantaneous thickness can be obtained from [4,5]

$$h_i = \frac{R_d^2 h_0}{R_d^2 + h_d^2} \tag{10}$$

p : Forming pressure (N/mm^2)

R : Radius of curvature (mm)

R_d : Die radius (mm)

h_d : Dome height (mm)

h_i : Instantaneous thickness (mm)

σ_1 : Circumferential stress (N/mm^2)

σ_2 : Tangential stress (N/mm^2)

σ_3 : Radial stress (N/mm^2)

σ : Equivalent stress (N/mm^2)

$$\frac{\sigma_1}{\sigma_2} = \frac{K\dot{\varepsilon}_1^m}{K\dot{\varepsilon}_2^m} \tag{10}$$

$$\frac{\sigma_1}{\sigma_2} = \left(\frac{\dot{\varepsilon}_1}{\dot{\varepsilon}_2}\right)^m \tag{11}$$

$$m = \frac{\log \dfrac{\sigma_1}{\sigma_1}}{\log \dfrac{\dot{\varepsilon}_1}{\dot{\varepsilon}_2}} \tag{12}$$

Table 7 Material properties for AA6061-T6 at 450°C

Variable	Value
Young's modulus (N/mm^2)	71000
Poisson's ratio	0.3
Material constant (Mpa s^m)	424
Strain-rate sensitivity	0.34
Friction coefficient	0.1

The hot tensile test performed for the FSW joints along the welded joint is used in the above Fig. 13 to determine the material constant m and K.

6. Finite Element Model

Superplastic forming is a complicated process involving large strain, large deformation, material non-linearity and usually deformation dependent boundary conditions [3]. Consequently, the numerical analysis of such a highly non-linear system involves difficulty in computation of the problems. The superplastic behaviour of materials is characterized by the dependency of the flow stress upon the strain-rate, which allows the material to be described as rigidviscoplatic. The simulation of superplastic forming can be performed ABAQUS.

The equivalent strain-rate is obtained from the constitutive equation

$$\sigma = K\dot{\varepsilon}^m \qquad (12)$$

The sheet and die configuration is shown in Fig.14 (a,b,c), before forming, during forming and after forming, respectively.

Finite Element simulations for the hemispherical dome shape are conducted in the study. The forming region of the die is 27 mm in diameter, and the initial sheet thickness is 2 mm. The die is defined as rigid body (R3D3 type) and sheet as a deformable body (S4R element) with axi-symmetric shell elements. The material is assumed to be isotropic, following the von Mises flow rule. A rigid-viscoplastic Finite Element Modelling for simulating Superplastic Forming processes was developed. The model is based on an incremental deformation theory, which assumes a minimum plastic-work path during a small time interval Δt. As an application to axisymmetric modeling, a hemisphere cup shape was simulated. Due to symmetry, only one half of the shape was modeled using 3 dimensional shell element. The predicted sheet thickness distribution for the Friction Stir Welded – Superplastic Forming specimens was simulated at pressure cycle for constant friction coefficients as shown in Fig. 15.

The blank sheet (deformable body) was clamped all around the edge as shown in Fig. 16. While the rigid body was encastred at the reference point as indicated. The deformable body was encastred at the edge which contact the die. The blank corner along the z-axis was locked. The interaction property was provided between master (rigid body) and slave (deformable body) as Surface-to-Surface contact with Finite Sliding and node to surface. The contact interaction property was initiated with tangential behavior, penalty method, friction coefficient as 0.1.

A total of 866 linear quadrilateral elements of type S4R are used to model the deformable body and the total of 506 linear triangular elements of type R3D3 are used to model the rigid body. Totally 1194 nodes and 1372 elements have been used for analysis. A very fine mesh is used in the Friction Stir Welded region (Zone 2) and coarse mesh is used in the non-welded region (Zone 1) shown in Fig.17. For a trail experiment, constant load is applied and the maximum strain rate is set to $3.36 \times 10^{-4} \text{s}^{-1}$ For all simulations, the analysis is done till the die height.
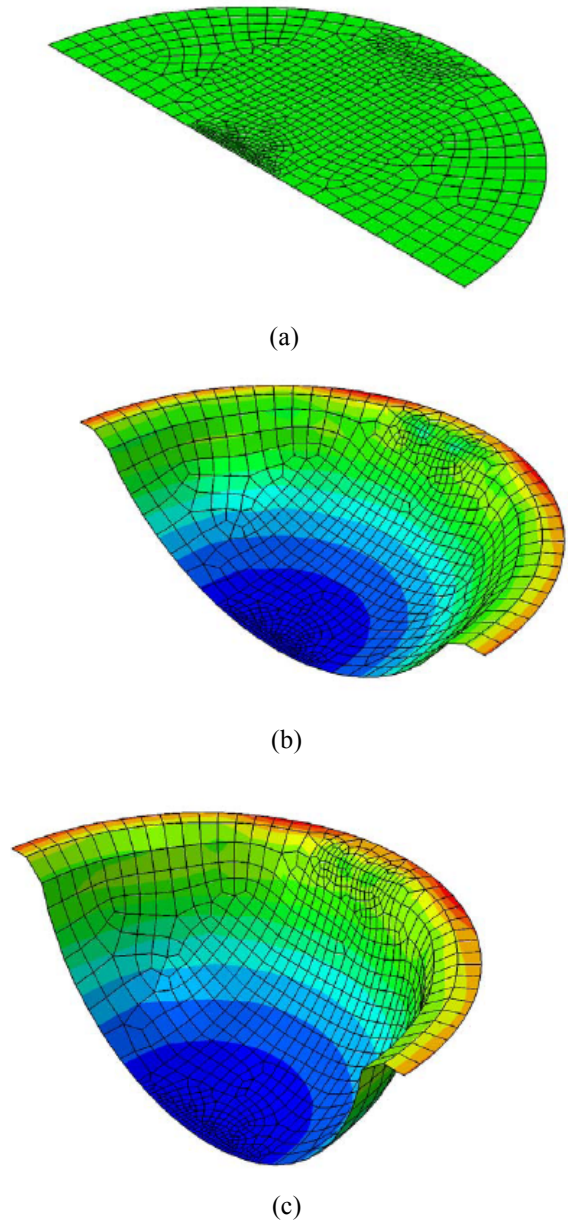

(a)

(b)

(c)

Fig. 14 The sheet and die configuration; (a) Before forming, (b) During forming and (c) After forming.
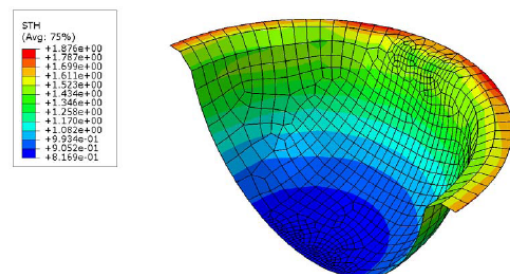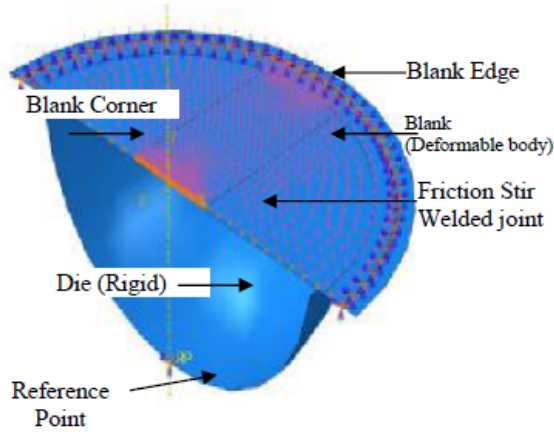

Fig. 15 Thickness Distribution.

Fig. 16 Selective Grain refinement.

A very fine mesh is used in the transition region between the fine and coarse grains to enhance the analysis accuracy [10]. The reason for using continuum elements is to capture the multiaxial stress state generated in the transition region. The load is controlled according to the maximum strain rate from the sheet, which is set to $3.36 \times 10^{-4} \, s^{-1}$.
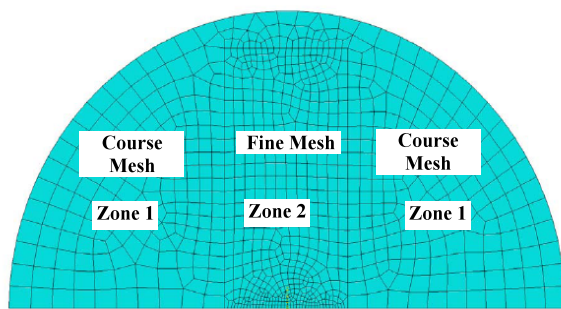

Fig. 17 Friction Stir Welded Blank with Zones 1 and 2 highlighted.

7. Results And Discussion

A finite element analysis using the shell element and a simple theoretical model has analyzed to compare the results with the existing experimental values.

The variation of relative bulge height with forming time at constant pressure is shown in Fig.18. It is observed that the dome height increases with constant pressure.
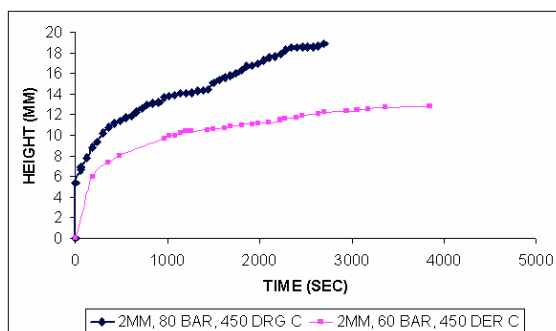

Fig. 18 Variation of bulge height with time.

The variation of the thickness during forming is shown in Fig.19. It is observed that the thickness of the component at the center is decreasing steadily during forming. Both theoretical and FEM model agrees fairly well.
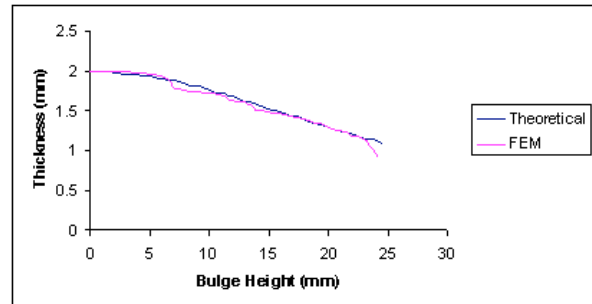

Fig. 19 Variation of thickness during forming.

8. Conclusion

In this paper, a experimental study of friction stir welded Superplastic forming of the AA6061-T6 sheets are formed through die forming. The experimental and finite element analyses have been conducted for optimum forming time and optimum temperature for the given pressure. The fine meshed area bulge profile increases during the forming with consequent decrease thickness at the pole. The formability for the FSW 1000 rpm showed a very high pole height than the other two welding speeds.

References

[1] F. Jovane, (1968), An approximate analysis of the superplastic forming of a thin circular diaphragm. Theory and experiments, Int. J. Mech. Sci., (10), p. 403–427.

[2] J.A. Belk, (1975), A quantitative model of the blow-forming of spherical surfaces in superplastic sheet metal, Met. Technol. (17), p. 505–511.

[3] V.S. Senthil Kumar, D. Viswanathan, S. Natarajan, (2006), Theoretical prediction and FEM analysis of Superplastic forming of AA7474 aluminium alloy in a hemispherical die, Int. J. Mat. Processing, (173), p. 247-251.

[4] Jung-Ho Cheng, (1994), A procedure for designing initial thickness variation for superplastic free inflation, Int. J. Mech. Sci., (11), p. 981-1000.

[5] Jung-Ho Cheng, (1996), The determination of material parameters from Superplastic inflation tests, J. mat. Proc. Tech., (58), p. 233-246.

[6] M. U. Polat, M. A. Dokainishi, (1990), A Finite Element Procedure for the Simulation of Superplastic Sheet Metal Forming Processes, Computers & Structures, (36) (2), p.251-259.

[7] Y. M. Hwang, J. S. Yang, T. R. Chen, J. C. Huang, (1997), Analysis of Superplastic sheet-metal forming

in a circular closed-die considering non-uniform thinning, J. Mat. Proc. Tech., (65), p. 215-227.

[8] Horng-tu-wu, Jiin-her Hwang, Chui-hung Chiu, (2009), Deformation characteristics and cavitation during multiaxial blow forming in superplastic 8089 alloy, J. Mat. Proc. Tech., (209), p. 1654-1661.

[9] T. Azimzadegan, S. Serajzadeh, An investigation into microstructures and mechanical properties of AA7075-T6 during friction stir welding at relatively high rotational speeds, J. Mat. Engg. Performance, DOI: 10.1007/s11665-010-9625-1.

[10] Mohammed A. Nazzal, Marwan K. Khraisheh, (2008), Impact of selective grain refinement on Superplastic deformation: Finite Element Analysis, J. Mat. Engg. performace, (17) (2), p. 163-167.

[11] Mohammed A. Nazzal, Marwan K. Khraisheh, Basil M. Darras, (2004), Finite element modeling and optimization of superplastic forming using variable strain rate approach, J. Mat. Engg. performace, (13) (6), p. 691-699.

[12] Karthikeyan L, Senthilkumar V.S; Padmanabhan K.A., (2010), On the role of process variables in the friction stir processing of cast aluminum A319 alloy. Mater. Des., (31), p. 761–771.